

Numerical study of a quantum spin in an s-wave superconductor using the natural orbitals renormalization group method

Wen-Jing Zhang(张文静), Ru Zheng(郑汝), Rong-Qiang He(贺荣强), and Zhong-Yi Lu(卢仲毅)
Citation: Chin. Phys. B, 2026, 35 (**2**): 027104. DOI: 10.1088/1674-1056/adf4af
http://cpb.iphy.ac.cn; http://iopscience.iop.org/cpb

What follows is a list of articles you may be interested in

Interacting Dirac semi-metal state in nonsymmorphic Kondo-lattice compound $CeAgSb_2$

Da-Liang Guo(郭达良), and Huan Li(黎欢)
Chin. Phys. B, 2025, 34 (**6**): 067102. DOI: 10.1088/1674-1056/adc6f6

Kondo screening cloud in a superconductor with mixed s-wave and p-wave pairing states

Zhen-Zhen Huang(黄真真), Xiong-Tao Peng(彭雄涛), Wan-Sheng Wang(王万胜), and Jin-Hua Sun(孙金华)
Chin. Phys. B, 2022, 31 (**10**): 107101. DOI: 10.1088/1674-1056/ac7213

Uniaxial stress effect on quasi-one-dimensional Kondo lattice $CeCo_2Ga_8$

Kangqiao Cheng(程康桥), Binjie Zhou(周斌杰), Cuixiang Wang(王翠香), Shuo Zou(邹烁), Yupeng Pan(潘宇鹏), Xiaobo He(何晓波), Jian Zhang(张健), Fangjun Lu(卢方君), Le Wang(王乐), Youguo Shi(石友国), and Yongkang Luo(罗永康)
Chin. Phys. B, 2022, 31 (**6**): 067104. DOI: 10.1088/1674-1056/ac6339

Intercalation of van der Waals layered materials: A route towards engineering of electron correlation

Jingjing Niu(牛晶晶), Wenjie Zhang(章文杰), Zhilin Li(李治林), Sixian Yang(杨嗣贤), Dayu Yan(闫大禹), Shulin Chen(陈树林), Zhepeng Zhang(张哲朋), Yanfeng Zhang(张艳锋), Xinguo Ren(任新国), Peng Gao(高鹏), Youguo Shi(石友国), Dapeng Yu(俞大鹏), Xiaosong Wu(吴孝松)
Chin. Phys. B, 2020, 29 (**9**): 097104. DOI: 10.1088/1674-1056/abab85

Benchmarking the simplest slave-particle theory with Hubbard dimer

Wei-Wei Yang(杨薇薇), Hong-Gang Luo(罗洪刚), Yin Zhong(钟寅)
Chin. Phys. B, 2019, 28 (**10**): 107103. DOI: 10.1088/1674-1056/ab3dfe

---

Numerical study of a quantum spin in an s-wave superconductor using the natural orbitals renormalization group method

Wen-Jing Zhang(张文静)[1], Ru Zheng(郑汝)[1,†], Rong-Qiang He(贺荣强)[2,3], and Zhong-Yi Lu(卢仲毅)[2,3,4,‡]

[1] *School of Physical Science and Technology, Ningbo University, Ningbo* 315211, *China*
[2] *School of Physics and Beijing Key Laboratory of Opto-electronic Functional Materials & Micro-nano Devices, Renmin University of China (RUC), Beijing* 100872, *China*
[3] *Key Laboratory of Quantum State Construction and Manipulation (Ministry of Education), Renmin University of China, Beijing* 100872, *China*
[4] *Hefei National Laboratory, Hefei* 230088, *China*

(Received 6 June 2025; revised manuscript received 25 July 2025; accepted manuscript online 28 July 2025)

In a superconductor embedded with a quantum magnetic impurity, the Kondo effect is involved, leading to the competition between the Kondo singlet phase and the superconductivity phase. By means of the natural orbitals renormalization group (NORG) method, we revisit the problem of a quantum magnetic impurity coupled with a conventional s-wave superconductor. Here we present a detailed study focusing on the impurity spin polarization and susceptibility, the Kondo screening cloud, as well as the number and structures of the active natural orbitals (ANOs). In the superconducting phase, the impurity spin is partially polarized, indicating that the impurity remains partially screened by the quantum fluctuations. Furthermore, the impurity spin susceptibility becomes divergent, resulting from the presence of residual local moment formed at the impurity site. Correspondingly, a non-integral (incomplete) Kondo cloud is formed, although the ground state is a spin doublet in this phase. In comparison, the Kondo cloud is complete in the Kondo singlet phase as expected. We also quantify the critical point, where the quantum phase transition from a Kondo singlet phase to a superconducting phase occurs, which is consistent with that in previous works. On the other hand, it is illustrated that only one ANO emerges in both quantum phases. The structures of the ANO, projected into both the real space and momentum space, are distinct in the Kondo singlet phase from that in the superconducting phase. More specifically, in the Kondo singlet phase, the ANO keeps fully active with half-occupied, and the superconducting gap has negligible influence on its structure. On the contrary, in the superconducting phase, the ANO tends to be inactive and its structure changes significantly as the superconducting gap increases. Additionally, our investigation demonstrates that the NORG method is reliable and convenient to solve the quantum impurity problems in superconductors as well, which will promote further theoretical studies on the Kondo problems in such systems using numerical methods.

Keywords: Kondo effect, superconductor, natural orbitals renormalization group, active natural orbitals

PACS: 71.10.–w, 71.10.Fd, 71.27.+a

DOI: 10.1088/1674-1056/adf4af **CSTR:** 32038.14.CPB.adf4af

1. Introduction

The Kondo effect[1,2] arises when a quantum impurity interacts with a normal metal, originated from the antiferromagnetic exchange interaction between the impurity and conduction electrons. Below the Kondo temperature $T_{\rm K}$, the impurity spin begins to be screened by surrounding itinerant electrons. Eventually, at zero temperature, a many-body spin singlet (or Kondo singlet) with the impurity spin being fully screened is formed, leading to a screening cloud spreading in real space with its spatial extension being determined by the Kondo length $\xi_{\rm K} = \hbar v_{\rm F}/k_{\rm B}T_{\rm K}$ ($v_{\rm F}$ denotes the Fermi velocity).[3–8] Many theoretical proposals[9–22] and experiments[23–28] have been devoted to detecting the Kondo screening cloud. Very recently, the Kondo cloud with a large extension in normal metals has been demonstrated via Fabry–Pérot oscillations in a mesoscopic system.[29]

On the other hand, the problem of a magnetic impurity embedded in a superconductor has been of extensive investigation for a very long time.[30–57] It was found that a localized excited state inside the superconducting gap, the Yu–Shiba–Rusinov (YSR) bound state (or Shiba state), is induced around the impurity by binding an anti-aligned quasiparticle from the superconductor.[30,32,33] The emergence of a pair of YSR states was theoretically predicted by the use of semiclassical approaches in the classical limit,[32] namely the impurity spin moment was treated as classical. However, when the magnetic impurity is described by quantum spin, the Kondo effect is involved.

For a local spin-1/2 antiferromagnetically coupled to a superconductor, a competition between the Kondo effect and the superconductivity arises, while the nature of the many-body ground state as well as the excited states are ultimately dominated by the ratio $T_{\rm K}/\Delta$ (Δ denotes the superconducting gap). In particular, for a weak Kondo coupling with

†Corresponding author. E-mail: zhengru@nbu.edu.cn
‡Corresponding author. E-mail: zlu@ruc.edu.cn

© 2026 Chinese Physical Society and IOP Publishing Ltd. All rights, including for text and data mining, AI training, and similar technologies, are reserved.

$T_K/\Delta \ll 1$, the Kondo effect is suppressed by the depletion of states upon the opening of the superconducting gap. In this case, the ground state is considered to take the form of a spin degenerate doublet with the impurity being unscreened, while the system exhibits a YSR singlet excitation within the energy gap.[37,50] In contrast, in the opposite limit of strong Kondo coupling with $T_K/\Delta \gg 1$, the Kondo effect occurs before the onset of superconductivity and the Kondo singlet becomes the ground state, while the localized excited state displays a doublet close to the energy gap.[36] Consequently, at zero temperature, by tuning the ratio of T_K/Δ, a first-order quantum phase transition from a free-spin doublet phase (superconducting phase) to a Kondo-screened singlet phase (Kondo phase) is predicted to take place at a critical point,[37,40,45,50,51,58] which is indicated to around $T_K/\Delta \approx 0.3$ by previous results from numerical renormalization group (NRG).[37]

Correspondingly, it is hence expected that the Kondo cloud is destroyed by the superconductivity in the doublet phase due to the lack of electrons at the Fermi level. Nevertheless, it is recently suggested that the Kondo cloud in a BCS s-wave superconductor, characterized by the correlation function between the impurity and the electrons, does exist in both quantum phases, while the screening is only partial in the doublet phase.[55] On the other hand, screening of the quantum impurity can be directly manifested by the spin of the impurity, especially the impurity spin polarization and susceptibility, while such studies suffer from a lack of reliable numerical calculations. Moreover, for the experimental implementation in tunable circuits of the Kondo effect, the state of the Kondo impurity and its progressive screening have been demonstrated to be directly observed.[59] Hence, in the superconductor, it is intriguing to investigate the Kondo cloud, as well as the screening of the quantum impurity described by the state of the impurity. In this work, we revisit the problem of a quantum magnetic impurity coupled with a conventional s-wave superconductor, notably from the perspective of the spin of the Kondo impurity. Additionally, we extend the application of natural orbitals renormalization group (NORG) method[60] that we used into the investigation of the quantum impurity problems in superconductors.

This paper is organized as follows. In Section 2 the model Hamiltonian and the NORG method we employed are introduced. In Subsections 3.1 and 3.2, we first study the local properties of the impurity, described by the zero-temperature spin polarization and spin susceptibility at the impurity site. In the following Subsection 3.3, the Kondo screening cloud, which is represented by the spin correlation between the impurity and the electrons, is further investigated. Additionally, at the end of the Subsection 3.3, we also extract the numerical value of the critical point $(T_K/\Delta)_c$, at which the quantum phase transition from a Kondo singlet phase to a spin doublet phase occurs. Finally, the number as well as the structures of the active natural orbitals (ANOs), which are helpful for clarifying the intrinsic structure of the many-body ground state, are analyzed in Subsection 3.4. Section 4 gives a summary of this work.

2. Model and numerical method

2.1. Model

We consider a conventional s-wave superconductor described by the general model Hamiltonian $H_{\rm BCS} = H_0 + H_\Delta$ in the BCS mean field theory with the following forms:

$$\begin{aligned} H_0 &= \sum_{k\sigma} \varepsilon_k (c^\dagger_{k\sigma} c_{k\sigma} + c^\dagger_{-k\sigma} c_{-k\sigma}), \\ H_\Delta &= \Delta \sum_k (c^\dagger_{k\uparrow} c^\dagger_{-k\downarrow} + c_{-k\downarrow} c_{k\uparrow}), \end{aligned} \tag{1}$$

where $c^\dagger_{k\sigma}$ creates an electron at a Bloch state with wavevector k and spin $\sigma = \uparrow, \downarrow$. The first term H_0 represents the kinetic energy of the electrons with the dispersion relation ε_k, and H_Δ describes the BCS pairing interaction with superconducting gap Δ. As we see, the charge $U(1)_{\rm charge}$ symmetry is broken by the superconducting pairing interaction H_Δ, namely, the total electrons in a superconductor is not conserved any more, while the z-component of the total spin is still conserved with $[S^z_{\rm total}, H_{\rm BCS}] = 0$.



Fig. 1. Sketch of an s-wave superconductor with the tight-binding chain emulation interacting with a Kondo impurity via antiferromagnetic exchange interaction. Δ is the superconducting gap and $J > 0$ the Kondo coupling strength. The spin-1/2 impurity is marked by the red dot and it interacts directly with the first site of the tight-binding chain.

We take the tight-binding chain emulation of the s-wave superconductor, as presented in Fig. 1, in which case the model Hamiltonian $H_{\rm BCS} = H_0 + H_\Delta$ is transformed into the forms as follows:

$$\begin{aligned} H_0 &= -t \sum_{i\sigma} (c^\dagger_{i\sigma} c_{i+1,\sigma} + \text{h.c.}), \\ H_\Delta &= \Delta \sum_i (c^\dagger_{i\uparrow} c^\dagger_{i\downarrow} + \text{h.c.}). \end{aligned} \tag{2}$$

Here, $c^\dagger_{i\sigma}$ ($c_{i\sigma}$) represents the creation (annihilation) operator of an electron at the ith site and t the hopping integral between the nearest-neighbor sites.

When a Kondo impurity interacts with the s-wave superconductor by antiferromagnetic exchange interaction, the total Hamiltonian is then obtained by $H = H_{\rm BCS} + H_{\rm Kondo}$ with

$$H_{\rm Kondo} = J \boldsymbol{S}_0 \cdot \boldsymbol{s}_1. \tag{3}$$

As schematically shown in Fig. 1, the impurity spin $\boldsymbol{S}_0$ is coupled to the electron spin $\boldsymbol{s}_1 = \frac{1}{2} \sum_{\alpha\beta} c^\dagger_{1\alpha} \boldsymbol{\sigma}_{\alpha\beta} c_{1\beta}$ at the first site via antiferromagnetic Kondo coupling $J > 0$ with $\boldsymbol{\sigma}$ representing the vector of Pauli matrices. The usual dimensionless

coupling is given by $j_0 = \rho_0 J$, here $\rho_0 = 1/\pi t$ is the density of states at the Fermi energy for the superconductor in the normal phase ($\Delta = 0$). Then the Kondo temperature is defined as $T_K = D\sqrt{j_0}\,e^{-1/j_0}$ for weak coupling with $j_0 \ll 1$, where $D = 2t$ denotes the half-bandwidth of conduction electrons. For a fixed Kondo coupling J, as the superconducting gap Δ increases from zero, it is predicted that a quantum phase transition will occur at a critical point Δ_c. In the case of $\Delta < \Delta_c$, the system is in the Kondo phase with the ground state being a Kondo singlet. On the contrary, in the regime of $\Delta > \Delta_c$, the system is in the superconducting phase and the ground state is a spin doublet.

On the other hand, for the total Hamiltonian H [Eqs. (2) and (3)], the total number of particles is not conserved, which makes our numerical simulation inconvenient. In order to avoid this technical inconvenience and employ the charge $U(1)_{\text{charge}}$ symmetry, we apply canonical transformations, a Bogoliubov transformation followed by a particle–hole transformation, to the total model Hamiltonian H. In specific, the performed Bogoliubov transformation takes the following forms:

$$b_{i\uparrow}^\dagger = \frac{1}{\sqrt{2}}(c_{i\uparrow}^\dagger + c_{i\downarrow}), \quad b_{i\downarrow} = \frac{1}{\sqrt{2}}(c_{i\uparrow}^\dagger - c_{i\downarrow}). \tag{4}$$

Under this transformation, the particles and holes combine into the Bogoliubov quasi-particles with $[b_{i\alpha}^\dagger, b_{j\beta}] = \delta_{ij}\delta_{\alpha\beta}$. Afterwards, we next perform the particle–hole transformation:

$$\begin{aligned} f_{2n,\uparrow}^\dagger &= b_{2n,\uparrow}^\dagger, \\ f_{2n,\downarrow} &= b_{2n,\downarrow}, \\ f_{2n-1,\uparrow}^\dagger &= b_{2n-1,\downarrow}, \\ f_{2n-1,\downarrow} &= -b_{2n-1,\uparrow}^\dagger, \end{aligned} \tag{5}$$

which makes an exchange between particle and hole for odd-number "site" while keep even-number "site" unchanged. Ultimately, we obtain the final expression of the total Hamiltonian $H = H_0 + H_\Delta + H_{\text{Kondo}}$ with

$$\begin{aligned} H_0 &= -t\sum_{i=1,\sigma}(f_{i\sigma}^\dagger f_{i+1,\sigma} + \text{h.c.}), \\ H_\Delta &= \Delta\sum_{i=1}(-1)^i(f_{i\uparrow}^\dagger f_{i\uparrow} + f_{i\downarrow}^\dagger f_{i\downarrow} - 1), \\ H_{\text{Kondo}} &= J\tilde{\boldsymbol{S}}_0 \cdot \tilde{\boldsymbol{s}}_1, \end{aligned} \tag{6}$$

where the impurity spin $\tilde{\boldsymbol{S}}_0 = \frac{1}{2}\sum_{\alpha\beta} f_{0\alpha}^\dagger \boldsymbol{\sigma}_{\alpha\beta} f_{0\beta}$ and the electron spin $\tilde{\boldsymbol{s}}_1 = \frac{1}{2}\sum_{\alpha\beta} f_{1\alpha}^\dagger \boldsymbol{\sigma}_{\alpha\beta} f_{1\beta}$ with $f_{0\sigma}^\dagger$ ($f_{1\sigma}^\dagger$) denoting the creation operator with spin σ at the impurity (first) site. Here, we can verify that $[f_{i\alpha}, f_{j\beta}^\dagger]_+ = \delta_{ij}\delta_{\alpha\beta}$ and $[f_{i\alpha}, f_{j\beta}]_+ = 0$. Therefore, for the final expression of H, the superconducting interaction H_Δ is transformed into a staggered potential without changing the total number of particles. As a result, we can thus block-diagonalize the total Hamiltonian H using both the conservation laws of the total number of particles and the z-component of the total spin.

2.2. Method

We used the NORG method (see Ref. [60] for details), a quantum many-body approach without perturbation, to study the Kondo problem in a superconductor. It has been demonstrated that the NORG method works efficiently on quantum impurity systems in the whole coupling regime and its effectiveness is independent of any topological structure of the systems. The NORG method has been successfully used to study the Kondo effect in several systems, such as the two-impurity or multichannel Kondo problem in normal metals[61–63] and that in quantum spin Hall insulators.[64–66] This work extends the application of NORG method to study the Kondo effect in superconductors.

Generally, realization of the NORG method involves a representation transformation through orbital rotations, namely from the original representation into the natural orbitals (NOs) representation. Therefore, the NORG method works in the Hilbert space constructed from a set of NOs, which are associated with the eigenvectors of the single-particle density matrix (or the correlation matrix).[60,67–73] On the other hand, the associated eigenvalues of the single-particle density matrix correspond to the occupancy numbers of the NOs. A natural orbital is called an ANO if its occupancy number deviates well from empty or full occupancy, otherwise an inactive orbital. In a quantum impurity system, it has been shown that the ANOs play substantial roles in constructing the ground-state wave function,[60,62,64,66] while the inactive NOs are frozen as background. The number of ANOs is roughly equal to that of the interacting impurities, which is the underlying basis for the NORG method working on quantum impurity problems.

Specifically, in a lattice system with finite size L, one performs the representation transformation via $d_m^\dagger = \sum_{i=1}^L U_{mi}^\dagger f_i^\dagger$, here $d_m^\dagger$ ($f_i^\dagger$) represents the corresponding creator in the NOs (site) representation and $U_{L\times L}$ is an unitary matrix diagonalizing the single-particle density matrix D defined by $D_{ij} = \langle\Psi|f_i^\dagger f_j|\Psi\rangle$ with $|\Psi\rangle$ a normalized many-body wave function of the system. In practice, to efficiently realize the NORG approach, we only rotate the orbitals of the bath, i.e., only the bath orbitals are transformed into NOs. As a result, the computational cost needed in the simulation is about $O(L^3)$ and hence we can solve hundreds of noninteracting bath sites with any topological structures.

In the following calculations, we set the hopping integral t as the energy unit with $t = 1.0$ and kept half-filling for the conduction band. Here the system size was $N = L + 1$ with $L = 4n$ denoting the size of tight-binding chain and the periodic boundary condition was adopted. All the calculations were carried out in the ground state subspace of $S_{\text{total}}^z = 1/2$.

3. Numerical results

3.1. Impurity spin polarization

Firstly, we study the static property of the local impurity, which is characterized by the impurity spin polarization $\langle S_0^z\rangle$ for the ground state. It is expected that the impurity spin will be mostly quenched (or fully screened) without polarization in the Kondo phase. On the contrary, in the case of $\langle S_0^z\rangle = 1/2$, namely the impurity is maximum polarized, the impurity spin is free without screened. Figure 2 presents the numerical result of $\langle S_0^z\rangle$, carried out in finite-size systems, with respect to the superconducting gap Δ for different Kondo couplings.

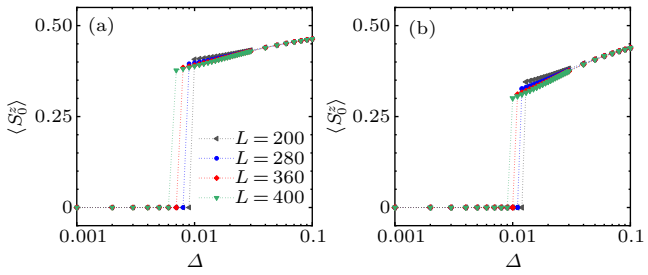


Fig. 2. The spin polarization $\langle S_0^z\rangle$ at the impurity site with different Kondo couplings (a) $J = 1$ and (b) $J = 1.2$ for the ground state. As expected, the impurity spin is not polarized with $\langle S_0^z\rangle$ vanishing in the regime of $\Delta < \Delta_c^L$, meaning that not free local moment is formed at the impurity site and the impurity is fully screened in the Kondo phase. When Δ further increases, $\langle S_0^z\rangle$ displays a jump to a finite value of $\langle S_0^z\rangle < 1/2$ at a critical superconducting gap Δ_c^L. Consequently, in the regime of $\Delta > \Delta_c^L$, the local spin is partially polarized, indicating that the impurity spin remains partially screened by quantum fluctuations in the spin doublet phase.

From Fig. 2, the impurity spin polarization vanishes with $\langle S_0^z\rangle = 0$ for small superconducting gap Δ, indicating that the impurity is no polarized and there is no free local moment formed at the impurity site in this case. However, as Δ further increases, $\langle S_0^z\rangle$ displays a jump to a non-vanishing value at a critical superconducting gap Δ_c^L depending on the system size L. Afterwards, when Δ goes beyond the critical point Δ_c^L, namely in the regime of $\Delta > \Delta_c^L$, $\langle S_0^z\rangle$ increases monotonously with $\langle S_0^z\rangle < 1/2$. This illustrates that in the case of $\Delta > \Delta_c^L$ in a finite-size system, the impurity spin is partially polarized with residual local moment formed at the impurity site.

Moreover, the finite-size effect modifies the behavior of the impurity spin polarization. Easily to see, the impurity spin polarization $\langle S_0^z\rangle$ always vanishes in the regime of $\Delta < \Delta_c^L$ for systems of different sizes we calculated, meaning that the impurity spin is fully screened in the Kondo phase as expected. In comparison, in the regime of $\Delta > \Delta_c^L$, the impurity spin polarization is inhibited by the system size L, as presented in Fig. 2 that the value of $\langle S_0^z\rangle$ at the critical point Δ_c^L decreases with L increasing. Consequently, in the thermodynamic limit $1/L \to 0$, the impurity spin polarization $\langle S_0^z\rangle$ is finite with $\langle S_0^z\rangle < 1/2$ in the regime of $\Delta > \Delta_c$ (Δ_c denotes the critical superconducting gap in the thermodynamic limit), indicating that the impurity spin is partially polarized in the superconducting phase. Hence, it is demonstrated that the impurity spin still remains partially screened by quantum fluctuations in the spin doublet phase.

3.2. Impurity spin susceptibility

In order to verify the above scenario, the spin susceptibility at the impurity site, representing dynamical property of the system, is further calculated. It is expected that the curve of impurity spin susceptibility with respect to the superconducting gap is discontinuous, in correspondence with the behavior of the impurity spin polarization.

We first consider the zero-temperature retarded Green's function $G_0(\omega + \mathrm{i}\eta)$ at the impurity site in the Lehmann representation,

$$G_0(\omega+\mathrm{i}\eta) = \langle 0|S_0^z \frac{1}{\omega+\mathrm{i}\eta - H + E_0} S_0^z|0\rangle, \tag{7}$$

where $|0\rangle$ and E_0 respectively represent the ground state and the ground-state energy. The spin-excitation spectral function at the impurity site $\chi_0(\omega)$ is then obtained by

$$\chi_0(\omega) = -\frac{1}{\pi}\lim_{\eta\to 0^+} \mathrm{Im}G_0(\omega+\mathrm{i}\eta), \tag{8}$$

and the zero-temperature impurity spin susceptibility χ_{loc} is further defined by

$$\chi_{\mathrm{loc}} = \chi_0(\omega = 0). \tag{9}$$

In our simulations, the spectral function $\chi_0(\omega)$ is calculated by the correction vector method[74,75] with a given Lorentzian broadening $\eta = t/L$. Our numerical results of the impurity spin susceptibility χ_{loc} for different Kondo couplings in finite-size systems are plotted in Fig. 3.

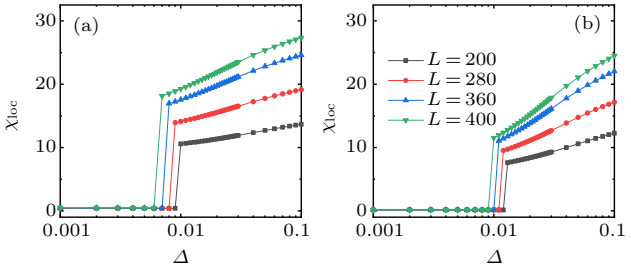


Fig. 3. The zero-temperature impurity spin susceptibility χ_{loc} calculated in finite-size systems for Kondo couplings (a) $J = 1$ and (b) $J = 1.2$ with the broadening factor $\eta = t/L$. In the regime of $\Delta < \Delta_c^L$, the susceptibility χ_{loc} vanishes as expected, meaning that the impurity is fully screened in the Kondo phase. As Δ increases, χ_{loc} jumps to a nonvanishing value at a critical superconducting gap Δ_c^L, consistent with the behavior of the impurity spin polarization. In the regime of $\Delta > \Delta_c^L$, the impurity spin susceptibility becomes finite rather than divergent.

As presented in Fig. 3, in the regime of $\Delta < \Delta_c^L$ (Δ_c^L depends on the system size L), the impurity spin susceptibility χ_{loc} vanishes as expected, meaning that the ground state is a spin singlet with the impurity spin being fully screened by the Kondo effect. As the superconducting gap Δ increases to a critical point Δ_c^L, χ_{loc} jumps to a nonvanishing value, consistent with the behavior of the impurity spin polarization as expected. Afterwards, in the regime of $\Delta > \Delta_c^L$, the impurity

spin susceptibility becomes finite rather than divergent, which is resulted from the finite-size effect.

Then we further determine the behavior of the impurity spin susceptibility in the thermodynamic limit in the superconducting phase. Note that the size-dependent broadening factor $\eta = t/L$ in our calculations decreases with increasing the system size L, and finally η vanishes in the thermodynamic limit $L \to \infty$. Figure 4 shows the zero-temperature spin-excitation spectra $\chi_0(\omega)$ and spin susceptibility $\chi_{\rm loc}$ at the impurity site calculated in different finite-size systems for $\Delta > \Delta_{\rm c}^L$ with Kondo coupling $J = 1$.

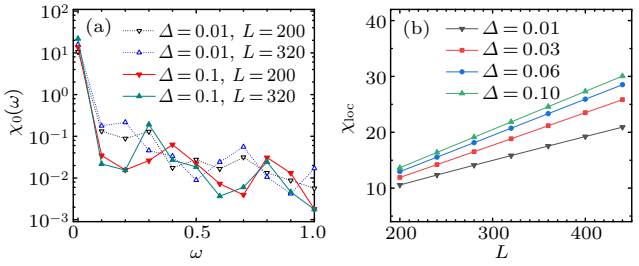


Fig. 4. (a) The zero-temperature spin-excitation spectra $\chi_0(\omega)$ for different system sizes and (b) the spin susceptibility $\chi_{\rm loc}$ as a function of the system size L at the impurity site. The numerical results are obtained using the broadening factor $\eta = t/L$ with the Kondo coupling $J = 1$. Our numerical results illustrate that the local spin susceptibility $\chi_{\rm loc}$ at the impurity site diverges in the superconducting phase in the thermodynamic limit.

From Fig. 4(a), in the case of $\Delta > \Delta_{\rm c}^L$, the spin-excitation spectra $\chi_0(\omega)$ increases as the frequency $\omega \to 0$, implying that the spin-excitation spectra $\chi_0(\omega \to 0)$ becomes divergent. On the other hand, for a fixed value of Δ with $\Delta > \Delta_{\rm c}^L$, $\chi_0(\omega \to 0)$ increases with the system size L, meaning that the spin-excitation spectra $\chi_0(\omega \to 0)$ tends to diverges for $\Delta > \Delta_{\rm c}$ in the thermodynamic limit. Moreover, as shown in Fig. 4(b), in the case of $\Delta > \Delta_{\rm c}^L$, the L dependence of $\chi_{\rm loc}$ reveals that $\chi_{\rm loc}$ increases linearly with the system size L, namely

$$\chi_{\rm loc} \propto L. \tag{10}$$

Hence, we can conclude that in the regime of $\Delta > \Delta_{\rm c}$

$$\lim_{L\to\infty} \chi_{\rm loc} \to \infty. \tag{11}$$

This demonstrates that the local spin susceptibility $\chi_{\rm loc}$ at the impurity site diverges in the superconducting phase in the thermodynamic limit, which is consistent with the behavior of the spin-excitation spectra $\chi_0(\omega \to 0)$. Here the divergent behavior of $\chi_{\rm loc}$ stems from the presence of residual local moment formed at the impurity site in the superconducting phase.

3.3. Kondo screening cloud

We proceed to study the Kondo screening cloud in the superconductor, which is manifested by the spin–spin correlation between the impurity and the conduction electrons. We introduce the integrity κ of the Kondo cloud as in Ref. [55], i.e., the screening ratio of the magnetic impurity, given by the following form:

$$\sum_i \langle \boldsymbol{S}_0 \cdot \boldsymbol{s}_i \rangle = -\frac{3}{4}\kappa. \tag{12}$$

Here $\langle \boldsymbol{S}_0 \cdot \boldsymbol{s}_i \rangle$ stands for the spin–spin correlation function between the impurity and the electrons at the ith site for the ground state. If the integrity $\kappa = 1$, this means a complete Kondo cloud is formed. Otherwise if $\kappa < 1$, the Kondo cloud is non-integral or incomplete. The numerical result of the integrity κ with respect to the superconducting gap Δ is plotted in Fig. 5.

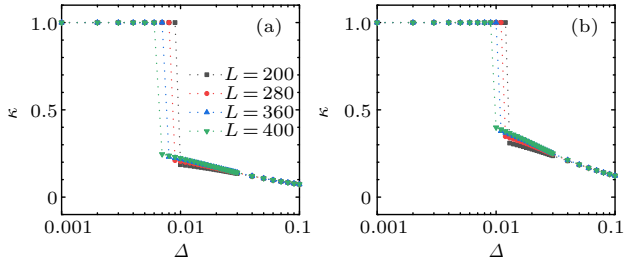


Fig. 5. The integrity κ of the Kondo cloud with respect to the superconducting gap Δ for the ground state with different Kondo couplings (a) $J = 1$ and (b) $J = 1.2$. The integrity $\kappa = 1$ for small superconducting gap Δ, meaning the Kondo cloud is complete in this regime. As Δ further increases and goes beyond a critical point $\Delta_{\rm c}$, κ exhibits a jump to a nonvanishing value of $\kappa < 1$. This demonstrates that the Kondo cloud is even formed in the superconducting phase, but it is non-integral with the impurity spin being partially screened, although the ground state is a spin doublet.

From Fig. 5, we can see that $\kappa = 1$ for small superconducting gap Δ, meaning the Kondo cloud is complete with the impurity being fully screened in this regime. As Δ further goes beyond a critical point $\Delta_{\rm c}^L$, κ exhibits a jump to a nonvanishing value of $\kappa < 1$, illustrating that a non-integral Kondo cloud is still formed around the impurity. Furthermore, the finite-size effect influences the behavior of the Kondo cloud. As presented in Fig. 5, in the regime of $\Delta \geq \Delta_{\rm c}^L$, the integrity κ is enhanced by the system size L. Consequently, in the thermodynamic limit $1/L \to 0$, κ becomes nonzero with $\kappa < 1$ in the case of $\Delta > \Delta_{\rm c}$ ($\Delta_{\rm c}$ represents the critical superconducting gap in the thermodynamic limit). Hence the Kondo cloud is even formed in the superconducting phase, but it is non-integral with the impurity spin being partially screened, although the Kondo singlet is not formed in this phase, which is in agreement with Ref. [55].

On the other hand, our numerical results illustrate that the integrity κ of the Kondo cloud is related to the impurity spin polarization $\langle S_0^z \rangle$ by the following form:

$$\kappa = 1 - 2\langle S_0^z \rangle, \tag{13}$$

and equation (13) holds in the whole regime of the Kondo coupling J. In particular, in the regime of $T_{\rm K} \gg \Delta$, i.e., in the Kondo singlet phase, the magnetic impurity is fully screened with $\langle S_0^z \rangle = 0$, leading to $\kappa = 1$.

To verify Eq. (13), we exploit the $\mathrm{U}(1)_{\mathrm{spin}}$ symmetry and the fact that the ground state $|0\rangle$ is an eigenstate of the total spin operator in the subspace of $S^z_{\mathrm{total}} = 1/2$, namely

$$S^z_{\mathrm{total}}|0\rangle = (S^z_0 + \sum_i s^z_i)|0\rangle = \frac{1}{2}|0\rangle. \tag{14}$$

Multiplying Eq. (14) by $\langle 0|S^z_0$ from the left and using the SU(2) symmetry with $\langle 0|(S^z_0)^2|0\rangle = 1/4$ and $\langle 0|S^z_0 s^z_i|0\rangle = (1/3)\langle 0|\boldsymbol{S}_0 \cdot \boldsymbol{s}_i|0\rangle$ yields immediately Eq. (13).

Nevertheless, when the calculations were carried out in the ground-state subspace of $S^z_{\mathrm{total}} = -1/2$, our numerical results (not shown) illustrate that

$$\kappa = 1 + 2\langle S^z_0\rangle, \tag{15}$$

with $\langle S^z_0\rangle$ the impurity spin polarization for the ground state in this case.

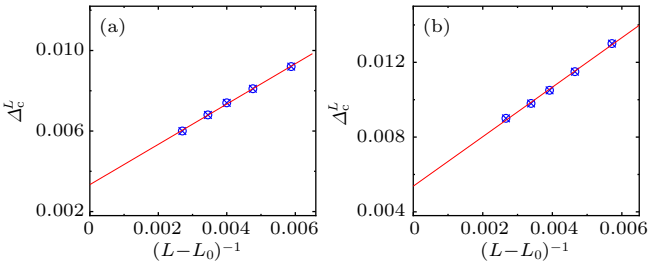


Fig. 6. The finite size extrapolation to the thermodynamic limit $L \to \infty$ of the critical superconducting gap Δ_c with different Kondo couplings (a) $J = 1$ and (b) $J = 1.2$. The line is determined by fitting Δ_c^L calculated in finite-size systems ($L = 200$, 240, 280, 320, and 400) with formula $\Delta_c^L = \Delta_c + a(L-L_0)^{-1}$, where Δ_c, a, and L_0 are fitting parameters depending on the Kondo coupling J. The fitting shows that $\Delta_c \approx 3.34 \times 10^{-3}$ with $L_0 = 30$ for the Kondo coupling $J = 1$ and $\Delta_c \approx 5.37 \times 10^{-3}$ with $L_0 = 25$ for $J = 1.2$.

Finally in this section, we quantify the critical superconducting gap Δ_c, at which point the quantum phase transition occurs. Our numerical results of Δ_c^L extracted from κ curves calculated for different values of L are plotted in Fig. 6. The value of Δ_c in the thermodynamic limit is obtained by the finite size extrapolation to $L = \infty$ by fitting, as presented by the curves in Fig. 6. The fitting shows that $(\Delta_c^L - \Delta_c) \propto (L-L_0)^{-1}$, where L_0 is a fitting parameter depending on the Kondo coupling J. Here, we emphasize that for moderate system sizes, the interacting quantum impurity modifies the behavior of the finite-size gap at the Fermi energy (which is proportional to $1/L$ for lager system sizes) as well as other quantities, a fitting parameter L_0 is thus introduced. From the fitting, we find that $\Delta_c \approx 3.34 \times 10^{-3}$ with $L_0 = 30$ for the Kondo coupling $J = 1$ and $\Delta_c \approx 5.37 \times 10^{-3}$ with $L_0 = 25$ for $J = 1.2$.

To compare with previous results from NRG, we further study the ratio T_K/Δ_c. Here the Kondo temperature T_K is defined as[3,16,76]

$$T_K = \mathcal{F}\, \mathrm{e}^{-\pi/c} \tag{16}$$

in the strong coupling regime, where $c = 2J/(1-3J^2/4)$ and $\mathcal{F}$ is a constant. Here, $\mathcal{F} = 1.5 \times 10^{-3}$ is determined numerically to fit the NRG results in Ref. [37] with $T_K/\Delta \approx 0.3$. Our numerical results show that the ratio $T_K/\Delta_c \approx 0.3$ for both Kondo coupings $J = 1$ and $J = 1.2$, indicating that the ratio $T_K/\Delta_c \approx 0.3$, which is consistent with the NRG results.[37] Hence, it is demonstrated that the quantum phase transition occurs around the critical point of $(T_K/\Delta)_c \approx 0.3$. In the case of $T_K/\Delta > 0.3$, the ground state is a Kondo singlet with the quantum impurity being fully screened. On the contrary, in the regime of $T_K/\Delta < 0.3$, the ground state is a spin doublet, while the impurity remains partially screened and a non-integral Kondo cloud is formed.

3.4. Active natural orbitals

As we have emphasized, in a quantum impurity system, the ANOs play essential roles in constructing the ground-state wave function, while the inactive NOs are frozen as background. In this section, we thus focus on the number as well as structures of the ANOs for the ground state, which are helpful for clarifying the intrinsic structure of the many-body ground state with strong correlation in such systems.

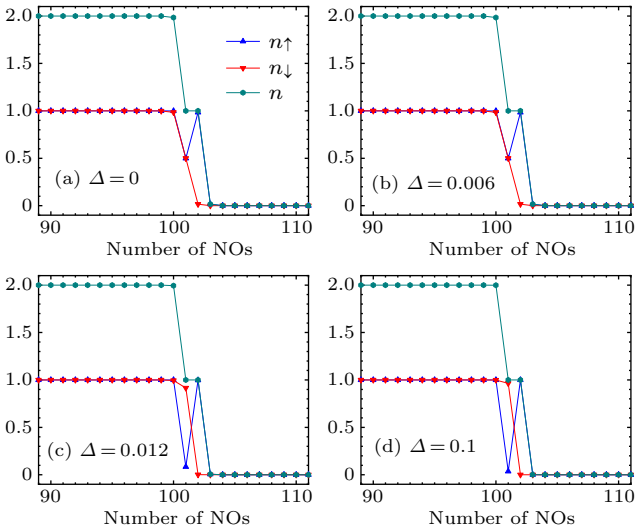


Fig. 7. Total occupancy number n ($0 \le n \le 2.0$) and the corresponding component n_σ ($0 \le n_\sigma \le 1.0$) of the NOs for the ground state with different values of the superconducting gap Δ. Here most of the NOs exponentially decay into full occupancy with $n = 2.0$ or empty with $n = 0$, except two NOs of half-occupied with $n = 1.0$. The corresponding component n_σ of the two NOs are further examined, and it is illustrated that only one NO can be identified as an ANO with n_σ deviates well from full occupancy or empty. The calculations were carried out in the system of size $L = 200$ with the Kondo coupling $J = 1$, in which the critical superconducting gap is around $\Delta_c^L \approx 0.009$.

In general, we identify an NO with both total occupancy number $n = n_\uparrow + n_\downarrow$ and the corresponding component n_σ deviating well from full occupancy or empty to be an ANO. Figure 7 shows the total occupancy number n ($0 \le n \le 2.0$) and the component n_σ ($0 \le n_\sigma \le 1.0$) of the NOs for different values of superconducting gap Δ. As we see, most of the NOs exponentially rush into full occupancy with $n = 2.0$ or empty with $n = 0$, meaning that they are inactive NOs. In comparisons, there are two NOs of half-occupied with total occupancy number $n = 1.0$, suggesting that there exist two candidates for

ANOs. We then further examine the corresponding component n_σ of the two NOs, and our results show that only one NO can be identified as an ANO with n_σ deviating well from full occupancy or empty. Hence, in this sense, only one ANO emerges for the ground state in the system of a conventional superconductor interacting with a Kondo impurity, being the same as that for the Kondo problem in a normal metal or a topological insulator.

On the other hand, the corresponding component n_σ of the ANO is expected to be affected by the superconducting gap Δ. More specifically, as presented in Figs. 7(a) and 7(b), in the regime of $\Delta < \Delta_c^L$ with $\Delta_c^L \approx 0.009$ for the system we calculated, the components $n_\uparrow$ and $n_\downarrow$ of the ANO are always hall-occupied with $n_\sigma = 0.5$, independent of the superconducting gap Δ. In comparisons, in the regime of $\Delta > \Delta_c^L$, as shown in Figs. 7(c) and 7(d), the component $n_\uparrow$ ($n_\downarrow$) tends to decrease (increase) to 0 (1.0) as the superconducting gap Δ increases, meaning that the ANO tends to be inactive. Therefore, the ANO keeps fully active with half-occupied in the Kondo phase, while it tends to be inactive as the superconducting gap Δ increases in the superconducting phase.

We proceed to clarify the structures of the ANO. To this end, we project it into the real space (site representation, namely Wannier representation) and momentum space, respectively. From the representation transformation $d_{m\sigma}^\dagger = \sum_{i=1}^L U_{mi\sigma}^\dagger f_{i\sigma}^\dagger$ ($d_{i\sigma}^\dagger$ represents the creation operator with spin σ at the i-th site in the NOs representation) involved in the realization of the NORG, we obtain the amplitude $w_{mi\sigma}$ of the m-th NO projected into the i-th Wannier orbital in the real space with $w_{mi\sigma} = |U_{mi\sigma}^\dagger|^2$. Similarly, the amplitude $\alpha_{mk\sigma}$ of the m-th NO projected into a Bloch state with wave vector k in the momentum space can be obtained by the Fourier transform of operators $f_{l\sigma}^\dagger = \frac{1}{\sqrt{L}}\sum_k \mathrm{e}^{-\mathrm{i}kl} f_{k\sigma}^\dagger$, and finally we get $\alpha_{mk\sigma} = |\frac{1}{\sqrt{L}}\sum_{l=1}^L \mathrm{e}^{-\mathrm{i}kl} U_{ml\sigma}^\dagger|^2$. The amplitudes $w_{i\sigma}$ and $\alpha_{k\sigma}$ of the ANO respectively projected into the real space and momentum space for different superconducting gaps are presented in Fig. 8.

From Figs. 8(a) and 8(b), in the regime of $\Delta < \Delta_c^L$ with $\Delta_c^L \approx 0.009$ for the system we calculated, we find that $w_{i\uparrow} = w_{i\downarrow}$ ($\alpha_{k\uparrow} = \alpha_{k\downarrow}$), meaning that the projection $w_{i\sigma}$ ($\alpha_{k\sigma}$) is spin-independent in this case. Furthermore, as we see, all the sites (Wannier orbitals) in the real space and all the single-particle states (low-energy excitations or higher energies) in the momentum space respectively participate to constituting the ANO, the same as that in a normal metal.[62] Additionally, our numerical results illustrate that the effect of the superconducting gap Δ on the structures of the ANO is negligible in this regime, as shown in Figs. 8(a) and 8(b) that the amplitudes $w_{i\sigma}$ and $\alpha_{k\sigma}$ for $\Delta = 0$ are nearly equivalent to those for $\Delta = 0.006$.

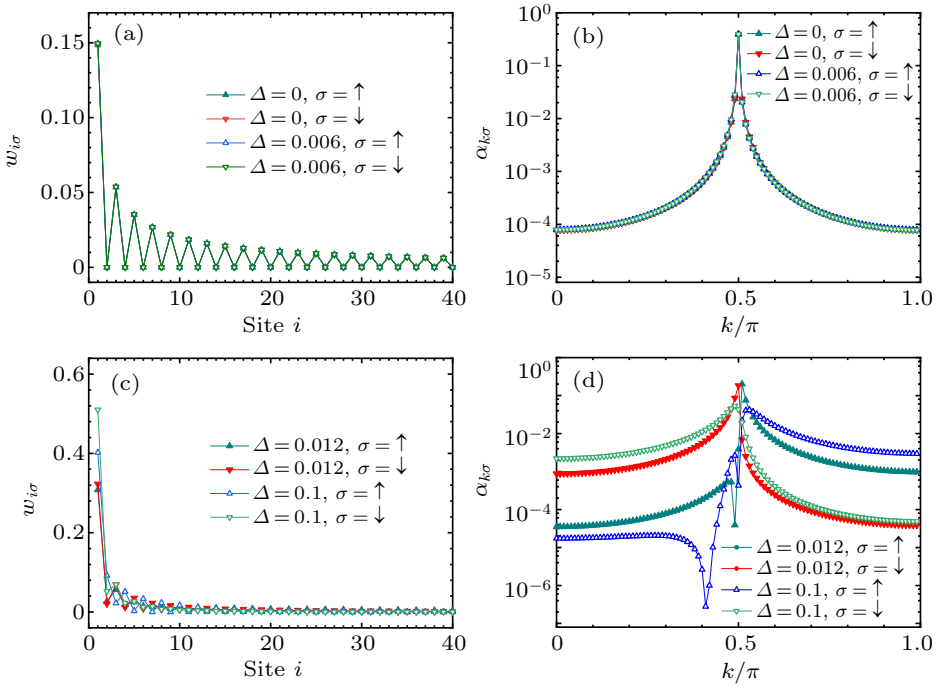


Fig. 8. The amplitudes $w_{i\sigma}$ and $\alpha_{k\sigma}$ of the ANO respectively projected into the real space and momentum space for different superconducting gaps. Structures of the ANO in the regime of $\Delta < \Delta_c^L$ is distinct from that in the regime of $\Delta > \Delta_c^L$. Our numerical results were obtained in the system of size $L = 200$ with the Kondo coupling $J = 1$ with the critical superconducting gap $\Delta_c^L \approx 0.009$. The Fermi energy of the tight-binding chain we used is $\varepsilon_{k_F} = 0$ with the Fermi wave vector $k_F = \pm\pi/2$, and the corresponding dispersion relation is given by $\varepsilon_k = -2t\cos(k)$.

When the superconducting gap Δ further increases and goes beyond the critical point Δ_c^L, the ANO displays different structures from that for $\Delta < \Delta_c^L$. As presented in Figs. 8(c) and 8(d), in the regime of $\Delta > \Delta_c^L$, the structures of the ANO are spin resolved with the amplitudes $w_{i\uparrow} \neq w_{i\downarrow}$ and $\alpha_{k\uparrow} \neq \alpha_{k\downarrow}$. Specifically, the amplitude $w_{1\sigma}$ of the ANO projected into

the first site, which couples directly with the magnetic impurity, becomes dominant, while the others decay dramatically with site i. This indicates that the ANO is localized in the real space. In the momentum space, the single-particle states above the Fermi energy dominantly compose the ANO for up spin with the amplitude $\alpha_{(k>\pi/2),\uparrow} \gg \alpha_{(k<\pi/2),\uparrow}$. On the contrary, the ANO for down spin is dominantly constituted by the single-particle states below the Fermi energy with the amplitude $\alpha_{(k<\pi/2),\downarrow} \gg \alpha_{(k>\pi/2),\downarrow}$.

Furthermore, we focus on the component that dominantly composes the ANO in the momentum space for $\Delta > \Delta_c^L$, namely the amplitudes $\alpha_{(k>\pi/2),\uparrow}$ and $\alpha_{(k<\pi/2),\downarrow}$. From Fig. 8(d), the projection $\alpha_{(k>\pi/2),\uparrow}$ [$\alpha_{(k<\pi/2),\uparrow}$] is enhanced by the superconducting gap Δ when the wave vector k deviates well from the Fermi wave vector $k_F = \pi/2$, while it is suppressed by Δ when k is near $k_F = \pi/2$. Consequently, as the superconducting gap increases, the weight of the single-particle states with up spin (down spin) above (below) the Fermi energy increases, while that around the Fermi energy decreases. Therefore, in the regime of $\Delta > \Delta_c^L$, structures of the ANO change significantly with the superconducting gap Δ increasing.

Hence in the system of a conventional superconductor interacting with a Kondo impurity, only one ANO emerges for the ground state, equal to the number of magnetic impurities. And our results clearly show that the structures of the ANO in the Kondo phase with $\Delta \ll T_K$ are distinct from that in the superconducting phase with $\Delta \gg T_K$. Specifically, in the Kondo phase, the ANO keeps fully active with half-occupied, and the superconducting gap has negligible influence on its structure. In contrast, in the superconducting phase, as the superconducting gap increases, the ANO tends to be inactive and its structure changes significantly.

4. Summary

In summary, using the NORG method, we have studied the problem of a quantum magnetic impurity coupled with a conventional s-wave superconductor. Here we presented a detailed study focusing on the impurity spin polarization and susceptibility, the Kondo screening cloud, as well as the number and structure of the ANOs.

We first considered the static and dynamical properties of the local impurity, characterized by the impurity spin polarization and spin susceptibility, respectively. Our numerical results clearly show that in the superconducting phase, the impurity spin is partially polarized, indicating that the quantum impurity remains partially screened by the quantum fluctuations, although the ground state is a spin doublet with the lack of electrons at the Fermi level in this phase. Furthermore, the impurity spin susceptibility tends to diverge, due to the presence of residual local moment formed at the impurity site.

Correspondingly, it is demonstrated that the Kondo cloud, manifested by the spin–spin correlation between the impurity and the conduction electrons, does exist in both quantum phases. In the Kondo phase, a complete Kondo cloud is formed as expected. In contrast, in the superconducting phase, the Kondo cloud becomes non-integral (incomplete) with the impurity being partially screened, even though that the Kondo effect is suppressed by the superconducting gap. Additionally, we quantified the critical point $(T_K/\Delta)_c \approx 0.3$, where the quantum phase transition from a Kondo phase to a superconducting phase occurs, which is consistent with previous NRG results.

Finally, the number and structure of the ANOs for the ground state were analyzed, which are helpful for clarifying the intrinsic structure of the many-body ground state with strong correlation in such systems. We show that only one ANO emerges in the system, equal to the number of the quantum impurities interacting with the superconductor. Structures of the ANO, which are distinct in the two different phases, are further displayed by their projections into the real space and momentum space. Specifically, in the Kondo phase, the ANO keeps fully active with half-occupied, and the superconducting gap has negligible influence on its structure. In contrast, in the superconducting phase, as the superconducting gap increases, the ANO tends to be inactive and its structure changes significantly.

On the other hand, our simulation shows that the NORG method is reliable and convenient to solve the quantum impurity problems in the superconductors as well, not limited to such problems in normal metals or topological insulators. Hence our investigation will promote further theoretical studies on the Kondo problems in the superconductor systems, such as in the topological superconductors, employing quantum many-body numerical methods.

Acknowledgements

Project supported by the National Natural Science Foundation of China (Grant Nos. 12104247 and 11934020). Computational resources were provided by Physical Laboratory of High Performance Computing at RUC.

References

[1] Kondo J 1964 *Prog. Theor. Phys.* **32** 37
[2] Hewson A C 1997 *The Kondo Problem to Heavy Fermions* (Cambridge: Cambridge University Press)
[3] Sørensen E S and Affleck I 1996 *Phys. Rev. B* **53** 9153
[4] Affleck I and Simon P 2001 *Phys. Rev. Lett.* **86** 2854
[5] Sørensen E S and Affleck I 2005 *Phys. Rev. Lett.* **94** 086601
[6] Bergmann G 2008 *Phys. Rev. B* **77** 104401
[7] Holzner A, McCulloch I P, Schollwöck U, von Delft J and Heidrich-Meisner F 2009 *Phys. Rev. B* **80** 205114
[8] Büsser C A, Martins G B, Costa Ribeiro L, Vernek E, Anda E V and Dagotto E 2010 *Phys. Rev. B* **81** 045111

[9] Gubernatis J E, Hirsch J E and Scalapino D J 1987 *Phys. Rev. B* **35** 8478
[10] Barzykin V and Affleck I 1996 *Phys. Rev. Lett.* **76** 4959
[11] Simon P and Affleck I 2002 *Phys. Rev. Lett.* **89** 206602
[12] Simon P and Affleck I 2003 *Phys. Rev. B* **68** 115304
[13] Hand T, Kroha J and Monien H 2006 *Phys. Rev. Lett.* **97** 136604
[14] Borda L 2007 *Phys. Rev. B* **75** 041307
[15] Affleck I, Borda L and Saleur H 2008 *Phys. Rev. B* **77** 180404
[16] Pereira R G, Laflorencie N, Affleck I and Halperin B I 2008 *Phys. Rev. B* **77** 125327
[17] Mitchell A K, Becker M and Bulla R 2011 *Phys. Rev. B* **84** 115120
[18] Yoshii R and Eto M 2011 *Phys. Rev. B* **83** 165310
[19] Park J, Lee S S B, Oreg Y and Sim H S 2013 *Phys. Rev. Lett.* **110** 246603
[20] Büsser C A, Martins G B and Feiguin A E 2013 *Phys. Rev. B* **88** 245113
[21] Shirakawa T and Yunoki S 2014 *Phys. Rev. B* **90** 195109
[22] Shirakawa T and Yunoki S 2016 *Phys. Rev. B* **93** 205124
[23] Boyce J B and Slichter C P 1974 *Phys. Rev. Lett.* **32** 61
[24] Boyce J B and Slichter C P 1976 *Phys. Rev. B* **13** 379
[25] Madhavan V, Chen W, Jamneala T, Crommie M F and Wingreen N S 1998 *Science* **280** 567
[26] Manoharan H C, Lutz C P and Eigler D M 2000 *Nature* **403** 512
[27] Fu Y S, Ji S H, Chen X, Ma X C, Wu R, Wang C C, Duan W H, Qiu X H, Sun B, Zhang P, Jia J F and Xue Q K 2007 *Phys. Rev. Lett.* **99** 256601
[28] Prüser H, Wenderoth M, Dargel P E, Weismann A, Peters R, Pruschke T and Ulbrich R G 2011 *Nat. Phys.* **7** 203
[29] Borzenets I V, Shim J, Chen J C H, Ludwig A, Wieck A D, Tarucha S, Sim H S and Yamamoto M 2020 *Nature* **579** 210
[30] YU L 1965 *Acta Phys. Sin.* **21** 75 (in Chinese)
[31] Soda T, Matsuura T and Nagaoka Y 1967 *Prog. Theor. Phys.* **38** 551
[32] Shiba H 1968 *Prog. Theor. Phys.* **40** 435
[33] Rusinov A I 1969 *Soviet J. Exp. Theor. Phys. Lett.* **9** 85
[34] Sakurai A 1970 *Prog. Theor. Phys.* **44** 1472
[35] Müller-Hartmann E and Zittartz J 1971 *Phys. Rev. Lett.* **26** 428
[36] Matsuura T 1977 *Prog. Theor. Phys.* **57** 1823
[37] Satori K, Shiba H, Sakai O and Shimizu Y 1992 *J. Phys. Soc. Jpn.* **61** 3239
[38] Sakai O, Shimizu Y, Shiba H and Satori K 1993 *J. Phys. Soc. Jpn.* **62** 3181
[39] Yazdani A, Jones B A, Lutz C P, Crommie M F and Eigler D M 1997 *Science* **275** 1767
[40] Balatsky A V, Vekhter I and Zhu J X 2006 *Rev. Mod. Phys.* **78** 373
[41] Bauer J, Oguri A and Hewson A C 2007 *J. Phys.: Condens. Matter* **19** 486211
[42] Karrasch C, Oguri A and Meden V 2008 *Phys. Rev. B* **77** 024517
[43] Ji S H, Zhang T, Fu Y S, Chen X, Ma X C, Li J, Duan W H, Jia J F and Xue Q K 2008 *Phys. Rev. Lett.* **100** 226801
[44] Luitz D J and Assaad F F 2010 *Phys. Rev. B* **81** 024509
[45] Franke K J, Schulze G and Pascual J I 2011 *Science* **332** 940
[46] Sau J D and Demler E 2013 *Phys. Rev. B* **88** 205402
[47] Yao N Y, Glazman L I, Demler E A, Lukin M D and Sau J D 2014 *Phys. Rev. Lett.* **113** 087202
[48] Yao N Y, Moca C P, Weymann I, Sau J D, Lukin M D, Demler E A and Zaránd G 2014 *Phys. Rev. B* **90** 241108
[49] Žitko R, Lim J S, Lǿpez R and Aguado R 2015 *Phys. Rev. B* **91** 045441
[50] Hatter N, Heinrich B W, Ruby M, Pascual J I and Franke K J 2015 *Nat. Commun.* **6** 8988
[51] Lee E J H, Jiang X, Žitko R, Aguado R, Lieber C M and De Franceschi S 2017 *Phys. Rev. B* **95** 180502
[52] Zazunov A, Plugge S and Egger R 2018 *Phys. Rev. Lett.* **121** 207701
[53] Li L, Gao M X, Wang Z H, Luo H G and Chen W Q 2018 *Phys. Rev. B* **97** 064519
[54] Akkaravarawong K, Väyrynen J I, Sau J D, Demler E A, Glazman L I and Yao N Y 2019 *Phys. Rev. Res.* **1** 033091
[55] Moca C P, Weymann I, Werner M A and Zaránd G 2021 *Phys. Rev. Lett.* **127** 186804
[56] Mishra A, Simon P, Hyart T and Trif M 2021 *PRX Quantum* **2** 040347
[57] Pasnoori P R, Andrei N, Rylands C and Azaria P 2022 *Phys. Rev. B* **105** 174517
[58] Deacon R S, Tanaka Y, Oiwa A, Sakano R, Yoshida K, Shibata K, Hirakawa K and Tarucha S 2010 *Phys. Rev. Lett.* **104** 076805
[59] Piquard C, Glidic P, Han C, Aassime A, Cavanna A, Gennser U, Meir Y, Sela E, Anthore A and Pierre F 2023 *Nat. Commun.* **14** 7263
[60] He R Q and Lu Z Y 2014 *Phys. Rev. B* **89** 085108
[61] He R Q, Dai J and Lu Z Y 2015 *Phys. Rev. B* **91** 155140
[62] Zheng R, He R and Lu Z 2020 *Sci. China Phys. Mech. Astron.* **63** 297411
[63] Zheng R, He R Q and Lu Z Y 2021 *Phys. Rev. B* **103** 045111
[64] Zheng R, He R Q and Lu Z Y 2018 *Chin. Phys. Lett.* **35** 067301
[65] Zheng R, He R Q and Lu Z Y 2021 *Phys. Rev. B* **104** 235134
[66] Zheng R, He R Q and Lu Z Y 2023 *Phys. Rev. B* **107** 115149
[67] Löwdin P O 1955 *Phys. Rev.* **97** 1474
[68] Luo H G, Qin M P and Xiang T 2010 *Phys. Rev. B* **81** 235129
[69] Zgid D, Gull E and Chan G K L 2012 *Phys. Rev. B* **86** 165128
[70] Lin C and Demkov A A 2013 *Phys. Rev. B* **88** 035123
[71] Lu Y, Höppner M, Gunnarsson O and Haverkort M W 2014 *Phys. Rev. B* **90** 085102
[72] Fishman M T and White S R 2015 *Phys. Rev. B* **92** 075132
[73] Lu Y, Cao X, Hansmann P and Haverkort M W 2019 *Phys. Rev. B* **100** 115134
[74] Kühner T D and White S R 1999 *Phys. Rev. B* **60** 335
[75] Jeckelmann E 2002 *Phys. Rev. B* **66** 045114
[76] Andrei N, Furuya K and Lowenstein J H 1983 *Rev. Mod. Phys.* **55** 331